RMetS
Royal Meteorological Society

Dependence of tropical cyclone intensification rate on sea-surface temperature

Nina Črnivec, Roger K. Smith* and Gerard Kilroy
Meteorological Institute, Ludwig Maximilians University of Munich, Germany

*Correspondence to: R. K. Smith, Meteorological Institute, Ludwig Maximilians University of Munich, Theresienstr. 37, 80333 Munich, Germany. E-mail: roger.smith@lmu.de

The dependence of tropical cyclone intensification rate on the sea-surface temperature (SST) is examined in the prototype problem for tropical cyclone intensification on an f-plane using a three-dimensional, non-hydrostatic numerical model. The effects of changing the SST are compared with those of changing the latitude examined in a recent article. It is found that the dependence of intensification rate on latitude is largest when the SST is marginal for tropical cyclone intensification (26 °C) and reduces in significance as the SST is increased. Further, at a given latitude, intensification begins earlier and the rate of intensification increases with increasing SST, on account of a significant increase of surface moisture fluxes from the warmer ocean. These higher fluxes result in higher values of near-surface moisture and equivalent potential temperature, leading to a larger radial gradient of diabatic heating rate in the low to middle troposphere above the boundary layer. This larger radial gradient leads to a stronger overturning circulation, which in turn leads to a stronger radial import of absolute angular momentum surfaces and therefore more rapid spin-up. These arguments invoke the classical axisymmetric spin-up mechanism. Non-axisymmetric issues are touched upon briefly.

Key Words: tropical cyclones; hurricanes; typhoons; intensity; rapid intensification; sea-surface temperature

Received 7 September 2015; Revised 9 January 2016; Accepted 21 January 2016; Published online in Wiley Online Library 29 April 2016

1. Introduction

In a recent study, Smith *et al.* (2015a) investigated why numerical model simulations of tropical cyclones in a quiescent environment show a more rapid rate of intensification as the latitude is decreased. After considering a range of physical processes involved in the intensification of storms, it was shown that the dynamics of the frictional boundary layer is a key element in the explanation. In an azimuthally averaged view of the problem, the most prominent quantitative difference between three-dimensional, time-dependent simulations at 10°N and 30°N is the much larger diabatic heating rate and its radial gradient above the boundary layer at the lower latitude. These differences were attributed to the larger vertical velocity found through the troposphere at 10°N, because the heating rate itself is approximately proportional to the vertical velocity. Since differences in initial Convective Available Potential Energy (CAPE) between the two latitudes were found to be relatively small, the differences in vertical velocity must be due to differences in the vertical velocity exiting the boundary layer. The much larger radial gradient of diabatic heating at 10°N produces a larger radial inflow in the low and mid-troposphere, leading to an increase in the rate at which absolute angular momentum (M) surfaces are drawn inwards. Although the radial gradient of M is larger at 30°N than at 10°N, the much larger inflow at 10°N is sufficient to give the larger spin-up rate at this latitude. These arguments for the dependence of spin-up rate on latitude invoke the classical spin-up mechanism (Ooyama, 1969; Montgomery and Smith, 2014; Smith and Montgomery, 2015), together with a boundary-layer feedback mechanism linking the strength of the boundary-layer inflow to that of the diabatic forcing. It was shown that the foregoing differences greatly surpass the effects of rotational stiffness (inertial stability) and evaporative wind feedback that have been proposed in some prior explanations.

The question immediately arises: is there evidence of a latitudinal dependence in observations of tropical cyclones? The answer is a qualified yes. A comprehensive statistical analysis of Atlantic hurricanes by Kaplan and DeMaria (2003) indicates that a larger proportion of low-latitude storms undergo rapid intensification than storms at higher latitudes. The qualification is that, in a more recent study by Kaplan and DeMaria (2010), latitude did not feature as an explicit predictor in their updated statistical prediction scheme. Nevertheless, as discussed by Kaplan and DeMaria (2003) and in a more recent climatological study by Hendricks *et al.* (2010), there are several environmental properties affecting storm intensification: vertical shear and sea-surface temperature (SST) are additional effects that may be influencing the statistics. Since SST typically increases as the latitude decreases, the question arises as to whether this effect might overwhelm the effects discussed by Smith *et al.* (2015a) in relation to the observations. To address this question, we seek here to isolate and quantify the effect of SST on the rate of

intensification of storms in relation to the effect of changing the latitude.

The article is organized as follows. First, in section 2 we introduce the numerical model used and in section 3 we present the results of the calculations. A physical explanation for the dependence of tropical cyclone intensification rate on SST is offered in section 4, based on an axisymmetric perspective. Some issues associated with a drift in the far-field ambient sounding, especially at higher SSTs, are examined in section 5.1 and some non-axisymmetric aspects of the problem are discussed briefly in section 5.2. Further issues associated with the interpretation of the results are discussed in section 6. Conclusions are given in section 7.

2. The numerical model

The numerical model used for the study is different from that used by Smith *et al.* (2015a), namely version 16 of CM1, a non-hydrostatic and fully compressible cloud model (Bryan and Fritsch, 2002). Smith *et al.* (2015a) used a modified version of the Pennsylvania State University/National Center for Atmospheric Research mesoscale model (MM5). For this reason, we have sought here to reproduce and verify the results of Smith *et al.* (2015a), before going on to investigate the dependence of the intensification rate on SST. All in all, we discuss nine numerical simulations, having combinations of three different latitudes (10°N, 20°N, 30°N) and three different SSTs (26°C, 28°C, 30°C). The simulations relate to the prototype problem for tropical cyclone intensification, which considers the evolution of a prescribed, initially cloud-free axisymmetric vortex in a quiescent environment on an f-plane as articulated in Nguyen *et al.* (2008).

The calculations are performed using the three-dimensional configuration of the CM1 model, similar to that described by Persing *et al.* (2013): in particular, the equations are as detailed therein. The main characteristics are as follows.

(1) The domain is $3000 \times 3000\,\mathrm{km}^2$ in size, with 570 grid points in each horizontal direction.
(2) The inner part of the domain has dimensions $600 \times 600\,\mathrm{km}^2$, with a constant grid spacing of 3 km (this compares with the grid spacing of 5 km used by Smith *et al.*, 2015a).
(3) Beyond 600 km, the horizontal grid is gradually stretched to a spacing of 10 km at the outer edges in the horizontal directions.
(4) The domain has 40 vertical levels extending to a height of 25 km. The vertical grid spacing expands gradually from 50 m near the surface to 1200 m at the top of the domain.

The background thermodynamic state is based on the Dunion moist tropical sounding (Dunion, 2011). The prescribed initial vortex is axisymmetric and in thermal wind balance. The initial tangential wind speed has a maximum of $15\,\mathrm{m\,s^{-1}}$ at the surface at a radius of 100 km from the centre of circulation. This velocity decreases sinusoidally with height, becoming zero at a height of 20 km. Above this height, the tangential wind is set to zero. The balanced pressure, density and temperature fields consistent with this prescribed tangential wind distribution are obtained using the method described by Smith (2006).

To suppress the artificial reflection of internal gravity waves from the upper boundary, a Rayleigh damping layer is added at heights above 20 km. The e-folding time-scale for this damping is 5 min. Rayleigh damping is also applied within 100 km of the lateral boundaries, which are rigid walls.

The simple Rotunno-Emanuel (1987) water-only scheme with a $7\,\mathrm{m\,s^{-1}}$ terminal fall velocity of rain is used as a warm-rain convection scheme. For simplicity, ice microphysical processes and dissipative heating are not included. Radiative effects are represented by adopting a simple Newtonian cooling approximation with a time-scale of 12 h. Following Rotunno and Emanuel (1987), the magnitude of the cooling rate is capped at 2 K per day.

As in Smith *et al.* (2015a), interest is focussed on the initial period of vortex intensification, whereupon the calculations are carried out for a period of 3 days.

3. Results

We examine in subsection 3.1 the latitudinal dependence of intensification rate (denoted *IR*) for a series of fixed SSTs. Then, in subsection 3.2, we highlight the SST dependence of *IR* at a fixed latitude. An interpretation of these results is given in section 4.

3.1. Dependence on latitude for different SSTs

Figure 1 compares time series of maximum azimuthally averaged tangential wind speed, $v_{\max}$ and *IR* in a series of calculations for one of three different latitudes (10°N, 20°N, 30°N), combined with one of three different SSTs (26, 28, 30 °C). The intensification rate at time t is defined as the 24 h change in maximum azimuthally averaged tangential wind speed, i.e. $IR = v_{\max}(t + 24\,\mathrm{h}) - v_{\max}(t)$. The black solid horizontal line in each right panel indicates the threshold value of $15\,\mathrm{m\,s^{-1}\,day^{-1}}$. Values of *IR* exceeding this threshold are used to characterize rapid intensification, often abbreviated 'RI' (Kaplan and DeMaria, 2003).

Figures 1(a) and (b) show the time series of $v_{\max}$ and *IR* in the calculations with the lowest SST (26 °C). It can be seen that the intensification is more rapid when the latitude is decreased. After 72 h, $v_{\max}$ for the vortex at 10°N is approximately $37\,\mathrm{m\,s^{-1}}$. In contrast, at this time, $v_{\max}$ for the vortices at 20°N and 30°N is much less, with values of ∼27 and $\sim 20\,\mathrm{m\,s^{-1}}$, respectively. Only the vortex at 10°N has an intensification rate exceeding the criterion for RI. This RI period begins at about 28 h and lasts approximately 20 h. The intensification rates of the vortices at 20°N and 30°N attain maxima of 11 and $5\,\mathrm{m\,s^{-1}\,day^{-1}}$, respectively.

Figures 1(c)–(f) show the corresponding time series for SSTs of 28 and 30 °C. At these SSTs, all vortices undergo a period of RI and, as for the lowest SST, the intensification rate decreases with increasing latitude and the time at which RI begins occurs later. The vortices at 28 and 30 °C reach approximately the same* intensity after 72 h and this intensity increases with SST (about $50\,\mathrm{m\,s^{-1}}$ at 28 °C and $70\,\mathrm{m\,s^{-1}}$ at 30 °C). These results confirm and extend those of Smith *et al.* (2015a), where an explanation for the latitudinal dependence of vortex evolution was provided. In particular, the results show that the differences in the evolution of $v_{\max}$ at different latitudes for a given SST become less as the SST is increased.

3.2. Dependence on SST at different latitudes

We examine now the dependence of vortex intensification on SST at a fixed latitude. While the information on this dependence is contained in Figure 1, it may be helpful to reorder the curves in a way that highlights the dependence on SST, as in Figure 2. In contrast to the dependence on latitude at a fixed SST, it is seen that there is a strong SST dependence of intensification rate and the time at which RI commences at all latitudes. As might be expected, the intensification is more rapid as the SST is increased (see Figures 2(a), (c) and (e)). Moreover, the onset of RI occurs earlier (when it occurs at all) and the duration of RI is longer as the SST is increased. For this reason, the final intensity after

*As pointed out by Nguyen *et al.* (2008) and Shin and Smith (2008), there will be an intrinsic variability of vortex intensity in calculations that start from slightly perturbed initial conditions, on account of the stochastic nature of deep convection. Therefore, small differences between the intensity of two deterministic calculations of a few $\mathrm{m\,s^{-1}}$ should not be regarded as particularly significant.

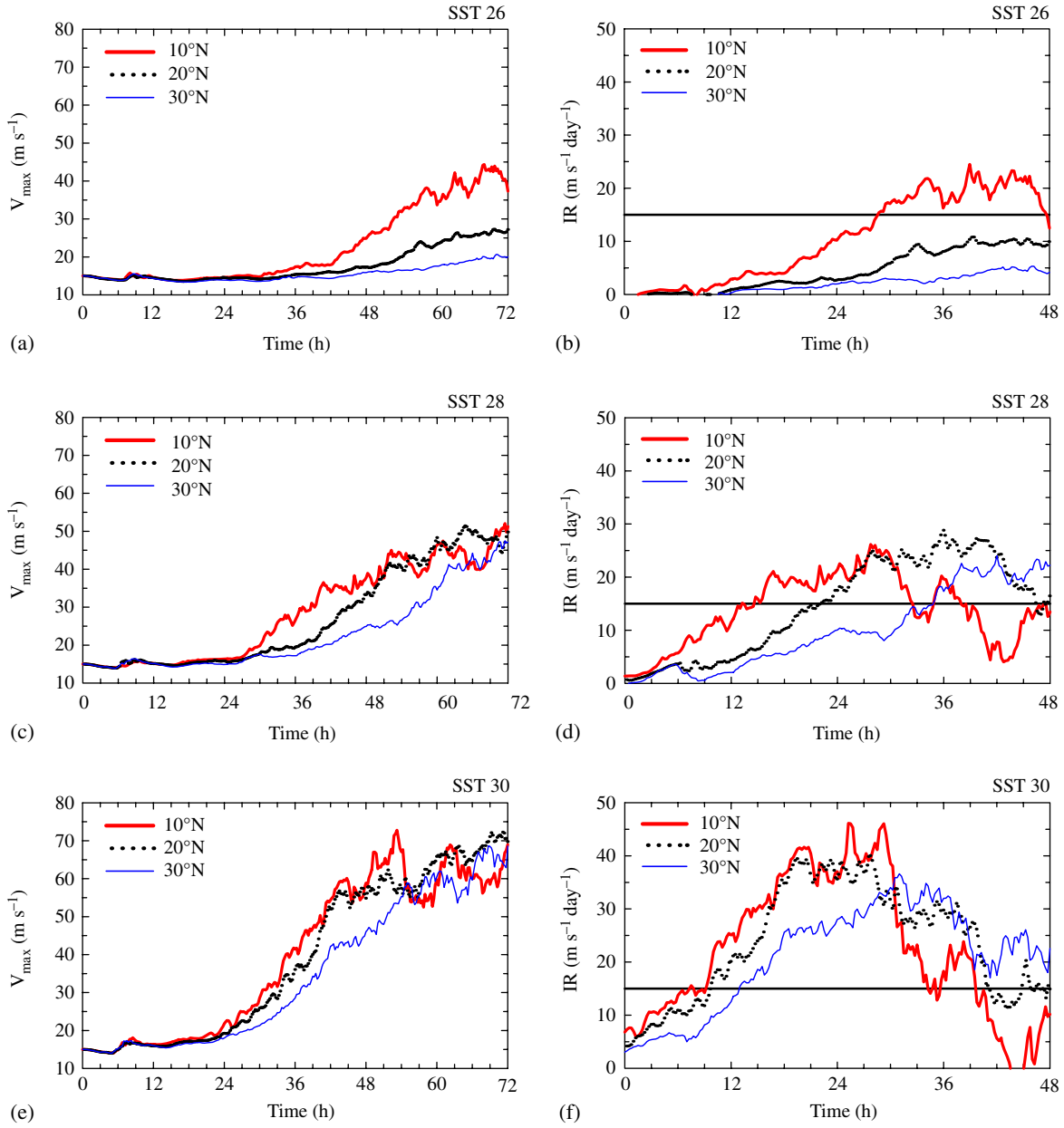

Figure 1. Time series of (a, c, e) maximum azimuthally averaged tangential wind speed and (b, d, f) intensification rate in the nine CM1 calculations at three different latitudes (10°N - thick solid red curve, 20°N - dotted black curve, 30°N - thin solid blue curve), combined with three different SSTs: (a, b) 26 °C, (c, d) 28 °C and (e, f) 30 °C. Note the difference in time period on the abscissa between the left and right panels.

3 days is greater for larger SSTs, although the difference is less at 10°N than at higher latitudes (possibly because the vortices at this latitude have achieved a greater degree of maturity). In the next section, we explore the reasons for the foregoing behaviour.

4. Interpretation of the SST dependence

4.1. *Boundary-layer moisture budget*

In the previous section, we sought to quantify the dependence of vortex intensification rate on SST at different latitudes compared with the *IR* dependence on latitude at a fixed SST. The aim, as outlined in the Introduction, was to assess the applicability of the results of Smith *et al.* (2015a) to explain Kaplan and DeMaria's (2003) observational climatology of RI. We showed that the intensification rate is substantially larger and that intensification begins sooner for larger values of SST. Here we examine why there is this strong dependence of intensification rate on SST. In seeking an explanation, the obvious place to start is to examine the differences in the azimuthally averaged latent heat fluxes as a function of radius and time. This is because the saturation specific humidity increases exponentially with temperature, implying a strong dependence of surface evaporation on the SST and a possibly greater disequilibrium in moisture at the sea surface.[†] Note that here we are not invoking the WISHE feedback mechanism (Montgomery *et al.* 2015).

The surface latent heat fluxes are shown in Figure 3 for all nine experiments. For a fixed SST the magnitude of the fluxes decreases with latitude and for a fixed latitude it decreases with decreasing SST, the dependence on SST being much stronger than that on latitude. Even so, as shown by Smith *et al.* (2015a), an elevation of latent heat flux does not necessarily lead to an increase in low-level moisture and thereby an increase in low-level equivalent potential temperature and CAPE. In their study, the amount of low-level moisture at 10°N is slightly less than that at 30°N, in spite of the larger surface evaporation at 10°N. They pointed out that stronger convection at 10°N is accompanied by stronger downdraughts, which bring dry air from aloft to the boundary layer, thereby decreasing the low-level moisture.

[†]In a bulk formulation, the moisture flux is proportional to the near-surface wind speed and the degree of disequilibrium, defined as the difference between the saturation specific humidity at the SST and the specific humidity of the near-surface air. Here, 'near-surface' is taken conventionally as 10 m altitude.

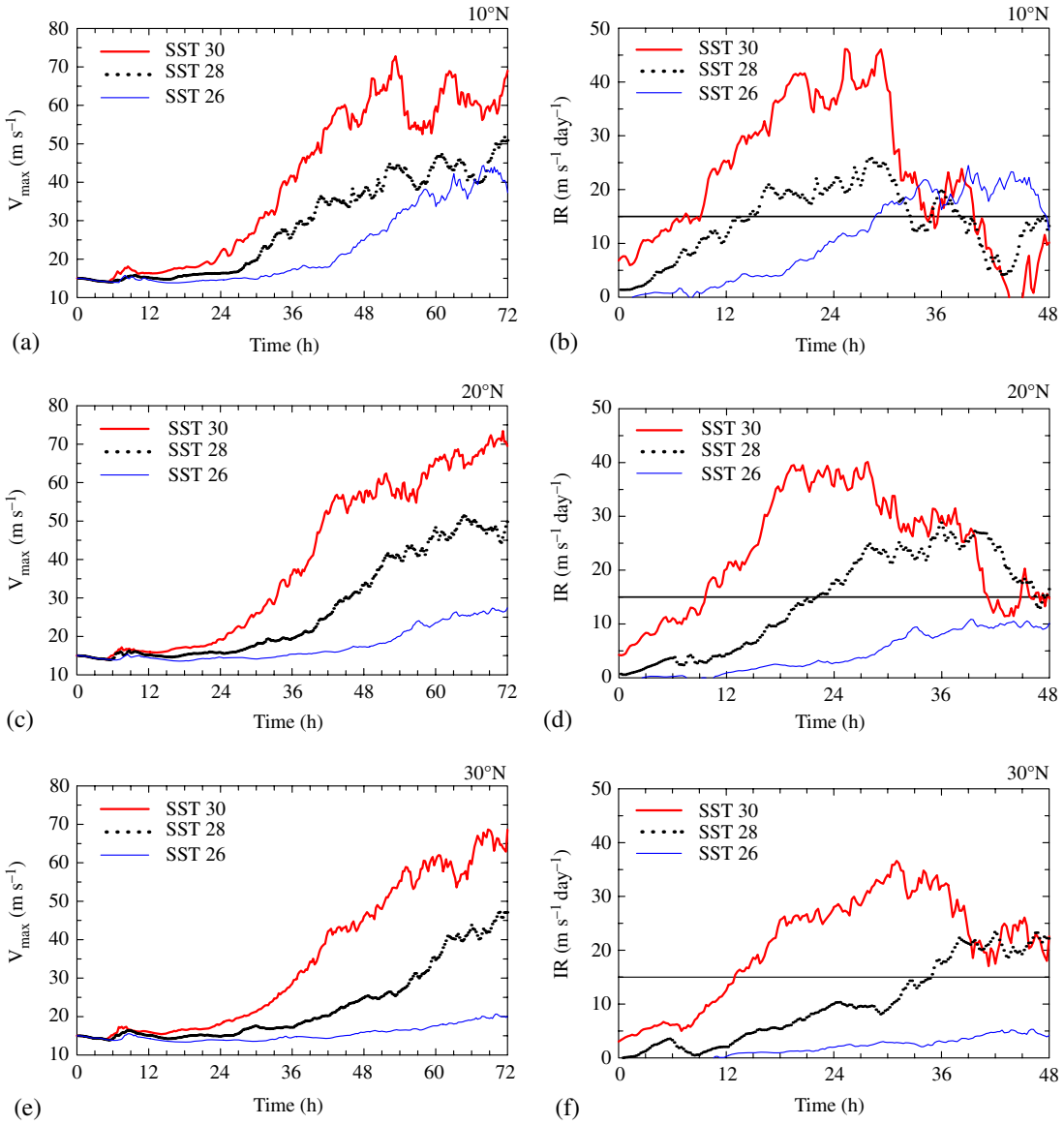

Figure 2. Time series of (a, c, e) maximum azimuthally averaged tangential wind speed and (b, d, f) intensification rate in the nine CM1 calculations with three different SSTs (26 °C - thin solid blue curve, 28 °C - dotted black curve, 30 °C - thick solid red curve) combined with three different latitudes: (a, b) 10°N, (c, d) 20°N and (e, f) 30°N . Note the difference in time period on the abscissa between the left and right panels.

We have examined the radius–time profiles of surface water-vapour mixing ratio at a given fixed latitude and found that values of the near-surface mixing ratio after ∼10–15 h, typically when deep convection first occurs, are slightly less than those initially in all nine experiments, in agreement with the results of Smith *et al.* (2015a). Nevertheless, at a particular latitude, the amount of moisture is still appreciably larger in the calculations with higher SSTs on account of the larger latent heat flux (not shown). These higher values of low-level moisture are reflected in larger values of equivalent potential temperature (θ_e), as indicated in Figure 4. This figure shows Hovmöller diagrams of azimuthally averaged θ_e at a height of 1.1 km for all nine experiments. We show here θ_e in preference to mixing ratio, because it not only increases monotonically with mixing ratio, but is an approximately conserved quantity also, both in dry and moist ascent. Moreover, its radial distribution as it exits the boundary layer is *one* important factor affecting the radial distribution of diabatic heating rate, the other being the radial distribution of vertical velocity at this level (see e.g. section 6 of Smith *et al.*, 2015b).

4.2. *Diabatic heating rate and secondary circulation*

Figure 5 shows the radius–time distribution of the azimuthally averaged diabatic heating rate, $\langle\dot{\theta}\rangle$, in the middle troposphere (at a height of 6 km) in the three simulations at latitude 20°N. There is clearly a strong dependence of $\langle\dot{\theta}\rangle$ on SST. As expected, the magnitude of $\langle\dot{\theta}\rangle$ and its radial gradient, $\partial\langle\dot{\theta}\rangle/\partial r$ (here r is the radius), are largest when the SST is 30 °C and weaken considerably as the SST is decreased. In accordance with the classical axisymmetric balance theory for intensification above the boundary layer, a stronger radial gradient of $\langle\dot{\theta}\rangle$ (a measure of the convective forcing in the balance theory for vortex intensification) leads to a stronger secondary circulation. In particular, a negative radial gradient of the diabatic heating rate leads to radial inflow in the lower troposphere at radii outside the heating (Shapiro and Willoughby, 1982). This inflow draws absolute angular momentum surfaces inwards above the boundary layer and, because M is approximately materially conserved above the boundary layer, the inflow leads to a spin-up of tangential wind speed there.

To quantify the foregoing effect in the context of balance dynamics, we first diagnose the spatial distribution of the time average of $\langle\dot{\theta}\rangle$ during a 3 h time interval surrounding the maximum value of *IR* for each of the three experiments (here the maximum *IR* is judged from a centred difference from $t - 12$ h to $t + 12$ h). The radius–height distributions of this average are shown in Figures 6(a)–(c) for the three calculations at 20°N with different SSTs. Again it is clear that there is a large difference in the mean heating rates between the calculations. The maximum

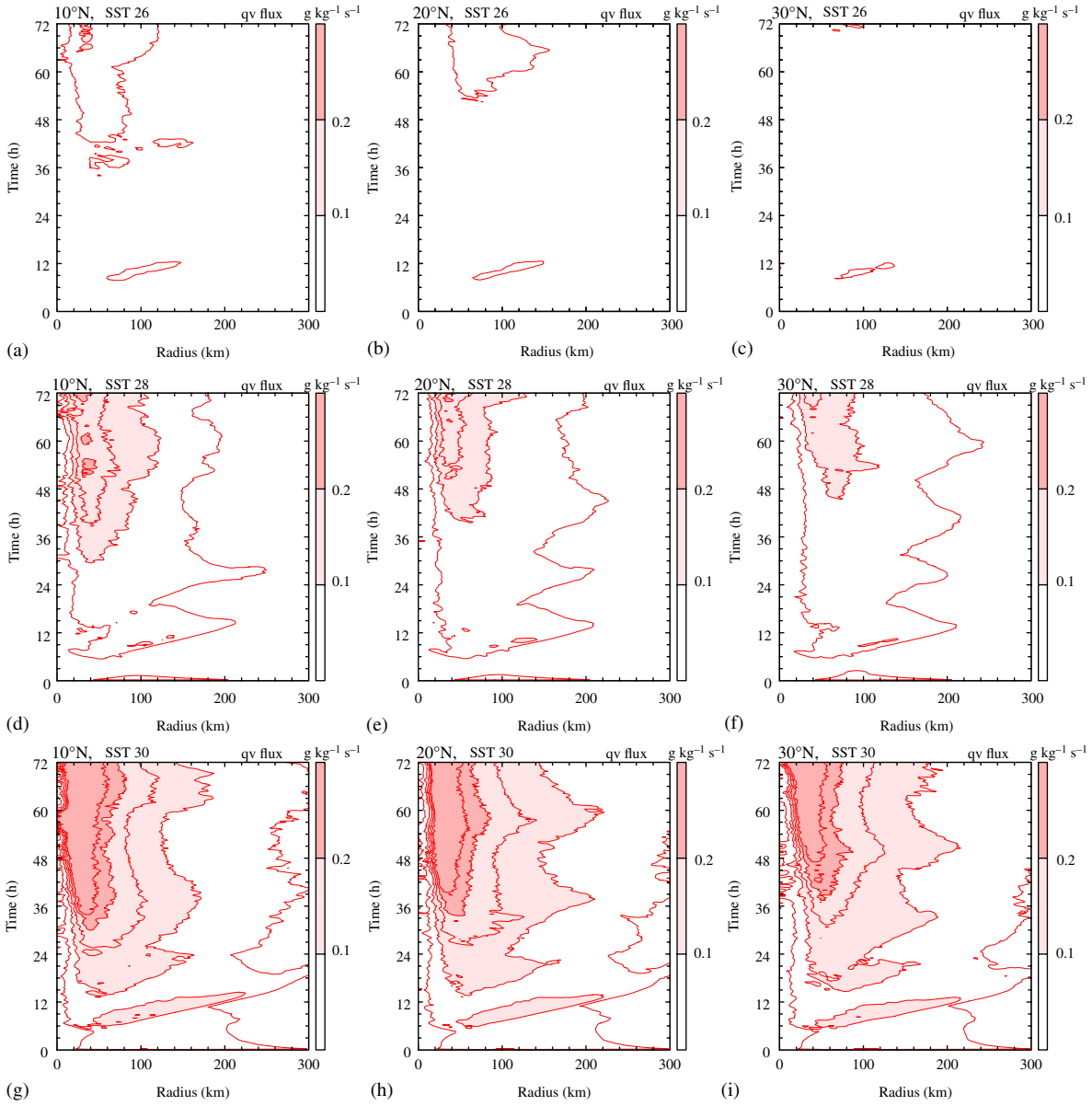

Figure 3. Radius–time plots of azimuthally averaged surface water vapour fluxes in the nine CM1 calculations at (a, d, g) 10°N, (b,e,h) 20°N and (c, f, i) 30°N for SSTs of (a–c) 26 °C, (d–f) 28 °C and (g–i) 30 °C. The contour interval is 0.05 g kg^{-1} s^{-1}, values between 0.1 and 0.2 g kg^{-1} s^{-1} are shaded light pink and values greater than 0.2 g kg^{-1} s^{-1} are shaded light red, as indicated in the colour bar.

values of $\langle\dot{\theta}\rangle$ reached in the calculations with SSTs of 26 °C, 28 °C and 30 °C are 11 K h^{-1}, 17 K h^{-1} and 22 K h^{-1}, respectively. Consistent with the behaviour of $\langle\dot{\theta}\rangle$ shown in Figure 5, the radial gradient of diabatic heating rate is considerably larger and its maximum is located closer to the storm axis in the calculation with the highest SST (30 °C), compared with other two calculations. Moreover, the vertical extent of high $\langle\dot{\theta}\rangle$ values (e.g., those exceeding 10 K h^{-1}) increases as the SST increases, leading to a deeper secondary circulation.

Panels (d), (e) and (f) of Figure 6 show isotachs of radial and vertical velocity in the balanced secondary circulation obtained by solving the Sawyer–Eliassen equation for the corresponding vortex and with the corresponding heating rate distribution from (a), (b) and (c) as forcing. Specifically, we solve Eq. (14) of Bui *et al.* (2009), neglecting both frictional forcing and the 'eddy terms'. The streamfunction contours of the overturning circulation are shown in these panels also. Confirming expectations, the balanced secondary circulation is strongest in the calculation with the highest SST (30 °C) and weakest in the calculation with the SST of 26 °C. In particular, the strongest vertical motion amounts to 1.1 m s^{-1} at 30 °C, while it is only 0.5 m s^{-1} at 26 °C. Similarly, the maximum low-level inflow velocity is 3.0 m s^{-1} for an SST of 30 °C, compared with 0.99 m s^{-1} in the calculation with the lowest SST (26 °C).

Panels (g), (h) and (i) in Figure 6 show isotachs of the tangential wind tendency in the three calculations. As might be expected, the largest positive low-level (below 2 km) tendency of the tangential wind is found in the calculation with the SST of 30 °C and amounts to 13.2 m s^{-1} h^{-1}. For an SST of 28 °C it is approximately 9.0 m s^{-1} h^{-1}, while at 26 °C it is only 1.6 m s^{-1} h^{-1}.

4.3. *Convective mass flux*

Another diagnostic quantity that can be used to quantify the degree of convective activity is the vertical mass flux averaged over some area of a storm. Of particular interest is the difference between the azimuthally averaged vertical mass flux at some middle tropospheric level and that near the top of the boundary layer. The sign of this difference provides an indication of the ability of deep convection to ventilate the air that is converging in the boundary layer. Moreover, the larger the difference, the stronger is the inflow above the boundary layer on grounds of mass continuity. In turn, the stronger the inflow above the boundary layer, the stronger will be the spin-up for a given radial gradient of absolute angular momentum in this region. This is essentially the classical (or conventional) spin-up mechanism, described in Montgomery and Smith (2014).

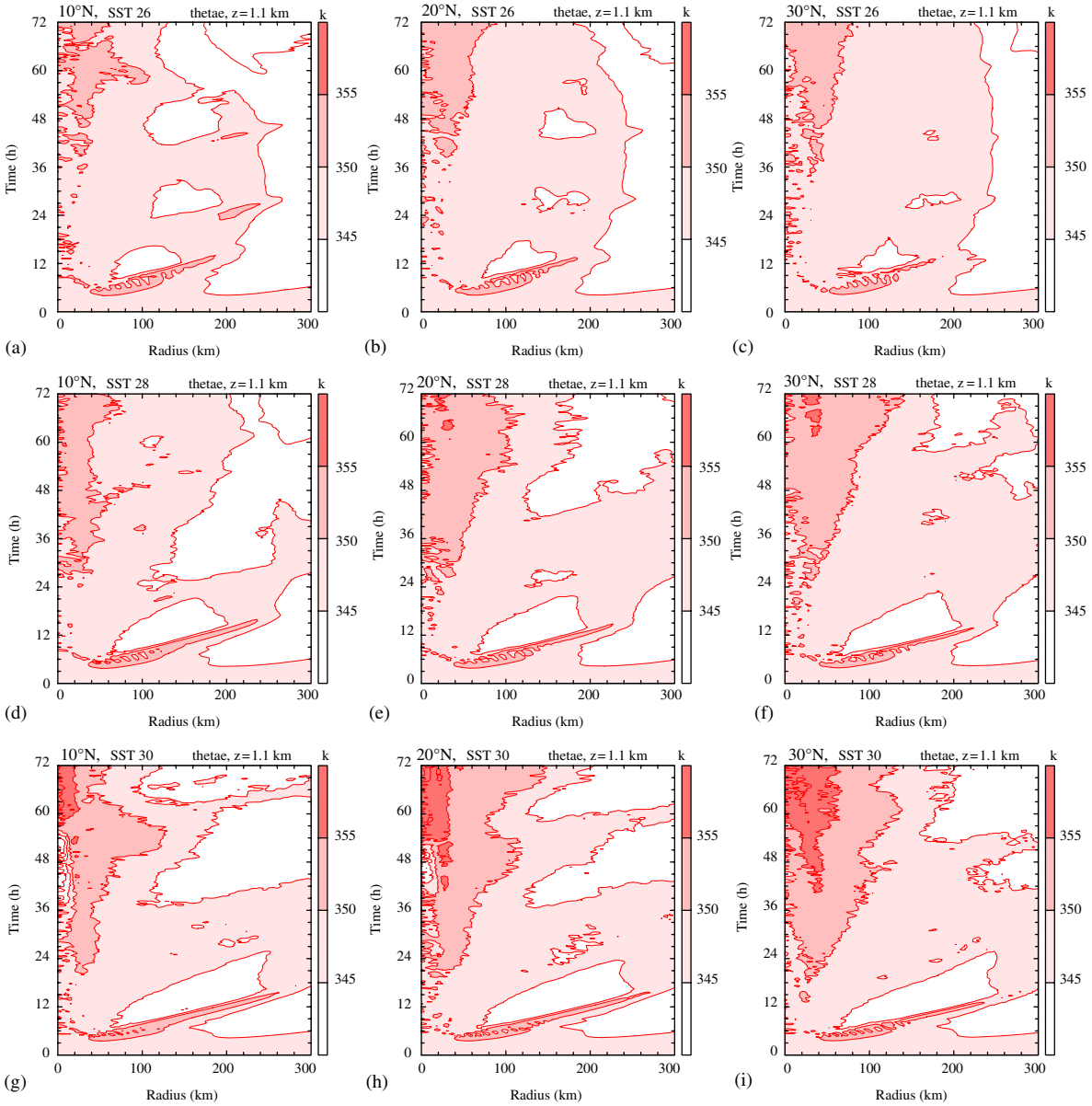

Figure 4. Radius–time plots of azimuthally averaged equivalent potential temperature at a height of 1.1 km in the nine CM1 calculations at (a, d, g) 10°N, (b,e,h) 20°N and (c, f, i) 30°N for SSTs of (a–c) 26 °C, (d–f) 28 °C and (g–i) 30 °C. The contour interval is 5 K. Shading is as indicated in the colour bar.

Figure 7 shows time series of the difference between the radially integrated mass fluxes at heights of 6.3 and 1.7 km in the three calculations at 20°N. Like ($\dot{\theta}$), this difference is largest when the SST is 30 °C and smallest when the SST is 26 °C. The implication is that there will be stronger spin-up above the boundary layer as the SST increases, consistent with the results shown at specific times during spin-up in section 4.2. Results for latitudes 10°N and 30°N are qualitatively similar (not shown). As anticipated, the convective mass flux difference is typically largest at the lowest latitude and decreases in magnitude when the latitude is increased.

5. Two remaining issues

We have shown that the dependence of vortex intensification on SST in the prototype problem for intensification may be understood in terms of the classical axisymmetric spin-up mechanism. However, there are two issues with the formulation and interpretation that need to be touched upon.

5.1. *Dependence of the ambient thermodynamic profile on SST*

There is a potential issue in carrying out experiments at a fixed latitude when varying the SST, but keeping the ambient sounding the same. In reality, the sounding itself may be expected to have some dependence on the SST. One could envision a set of experiments in which the initial sounding is adjusted so as to be neutral to the model's moist convection, as was done by Rotunno and Emanuel (1987, p. 548). One thrust of the Rotunno and Emanuel study was to demonstrate that tropical cyclone intensification does not require ambient CAPE. In essence, these authors showed that, starting from a prescribed initial vortex, the presence of wind-induced surface moisture fluxes generates adequate CAPE to support inner core deep convection.

Elsewhere, Emanuel *et al.* (1994) have argued that levels of CAPE over the tropical oceans are minimal, sufficient only to offset the dissipation within clouds, although they use a definition of CAPE that assumes reversible adiabatic displacements. This definition includes the effects of condensed water on air parcel buoyancy and applies strictly to non-precipitating convection. On the other hand, recent observations of the environment of tropical disturbances have shown that, based on the assumption of pseudo-adiabatic ascent, there are significant levels of CAPE (Smith and Montgomery, 2012). In the systems analyzed by Smith and Montgomery, approximately 50% of soundings had CAPE values exceeding 1500 J kg^{-1} and approximately 10% had values exceeding 2500 J kg^{-1}. These amounts would be adequate to support modes of convective organization, just as in the middle latitudes over land.

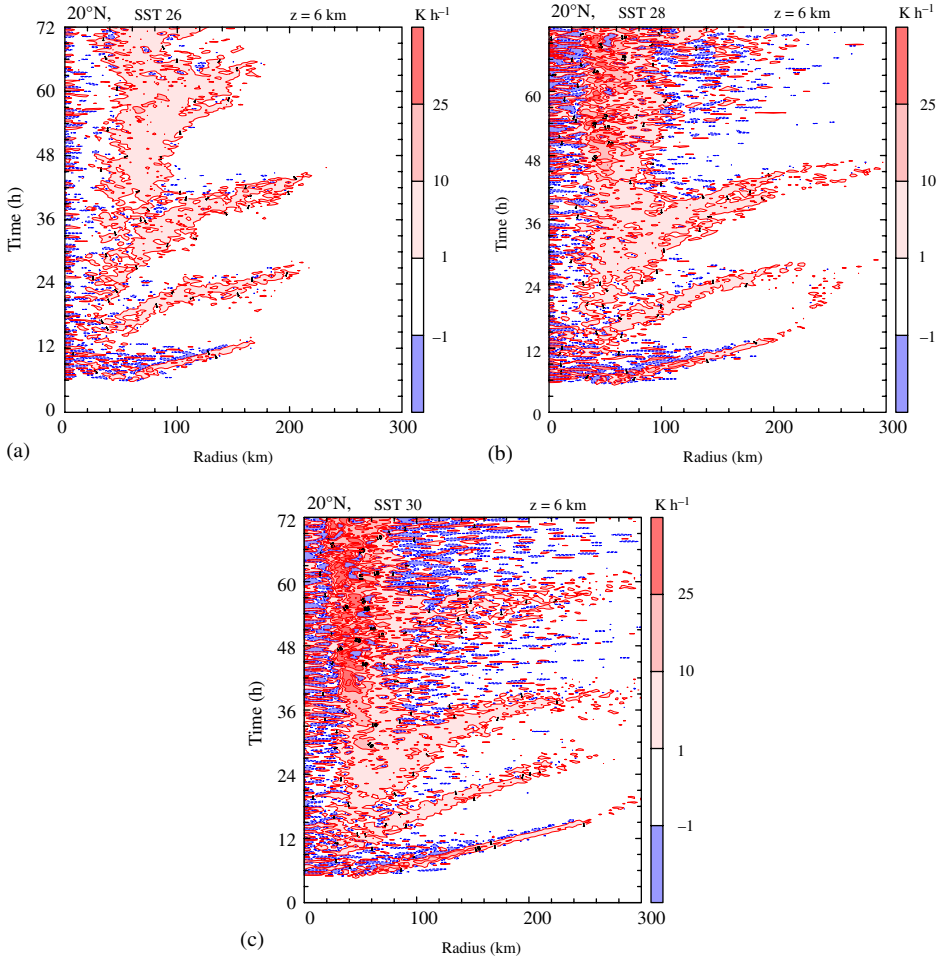

Figure 5. Hovmöller diagrams of azimuthally averaged diabatic heating rate at a height of 6 km in a series of CM1 calculations at 20°N for SST values of (a) 26 °C, (b) 28 °C and (c) 30 °C. Values between 1 and 10 K h^{-1} are shaded very light pink. Values between 10 and 25 K h^{-1} are shaded pink and values greater than 25 K h^{-1} are shaded red. The contour interval for thick red contours above 25 K h^{-1} is 25 K h^{-1}. Values lower than −1 K h^{-1} are shaded light blue.

An unavoidable consequence of changing the SST without changing the initial ambient profile is that the vertical diffusion of heat and moisture near the surface may lead to a slow evolution of the ambient sounding, thereby changing the level of ambient CAPE during the integration period. While this change may not be appreciable during the comparatively short integration period here, it is an effect that calls for investigation and quantification.

Figures 8(a)–(c) show the time evolution of the far-field potential temperature deviation (specifically the difference between θ at a radius of 1000 km at time t and that at the initial time) in the lowest 300 m in the three simulations for latitude 10°N. The lower panels (d)–(f) show the corresponding deviations in water-vapour mixing ratio in the lowest 1 km. One might expect the magnitude of the deviations to be most extreme at this latitude. As expected, the deviations of both quantities are largest when the SST is 30 °C and are almost imperceptible when the SST is 26 °C. Since the near-surface air temperature of the Dunion sounding (26.7 °C) exceeds 26 °C, θ actually decreases slightly with time when the SST is 26 °C and, because of the implied static stability, the decrease is confined to a very shallow layer of 50 m near the surface. In the calculations for SSTs of 28 °C and 30 °C, θ increases with time on account of the sensible heat fluxes from the warmer ocean surface. By 72 h, θ at the lowest model level has increased by about 1.2 K in the calculation with the highest SST (Figure 9(a)). In this most extreme case, an almost neutral layer develops in the lowest 300 m (specifically, the increase in θ across this layer reduces from 1.3 °C to less than 0.2 °C).

For all values of SST, there is an increase in the low-level moisture that extends through a deeper layer than the increase in potential temperature (up to about 1 km in the case of 30 deg SST), the maximum being of the order of 2 g kg^{-1} near the surface. The question is: what are the implications of these changes for the change in far-field values of CAPE? In the most extreme case, the average CAPE for the average vertical profile during the last 12 h period is about 500 J kg^{-1} higher than the initial value of approximately 2200 J kg^{-1}. The next question is: how significant is this increase in initial ambient CAPE? To answer this question, we repeated the calculation for an SST of 30 °C at a latitude of 10°N with the foregoing averaged profiles of temperature and moisture at the initial time. The differences in intensity evolution between this calculation and the original one are shown in Figure 9(b). Some small differences in the intensity evolution begin to appear after 24 h of integration, which is near the start of the RI phase. From the study of Nguyen *et al.* (2008), such differences are to be expected on account of the stochastic nature of deep convection in the model. Between 24 and 72 h, the standard deviation of the difference between the two intensity curves is ±2.5 m s^{-1}, which on the basis of Nguyen *et al.*'s results would be judged to be not significant.

5.2. *Non-axisymmetric features*

Satellite and radar observations indicate that tropical cyclones are highly asymmetric during their intensification phase and only in their mature stage do they exhibit a moderate degree of axial symmetry in their inner-core region (Montgomery and Smith, 2014). This is certainly true of the calculations described here, as exemplified by the patterns of vertical motion in the mid troposphere (at a height of 6.3 km) for an SST of 28 °C and latitude 20°N in Figure 10. At 48 h, the convection is organized in a partial ring (shown in (a)) and by 72 h the ring has begun to consolidate, while a band of outer convection has begun to form also (shown in (b)). Despite this lack of complete symmetry, the arguments

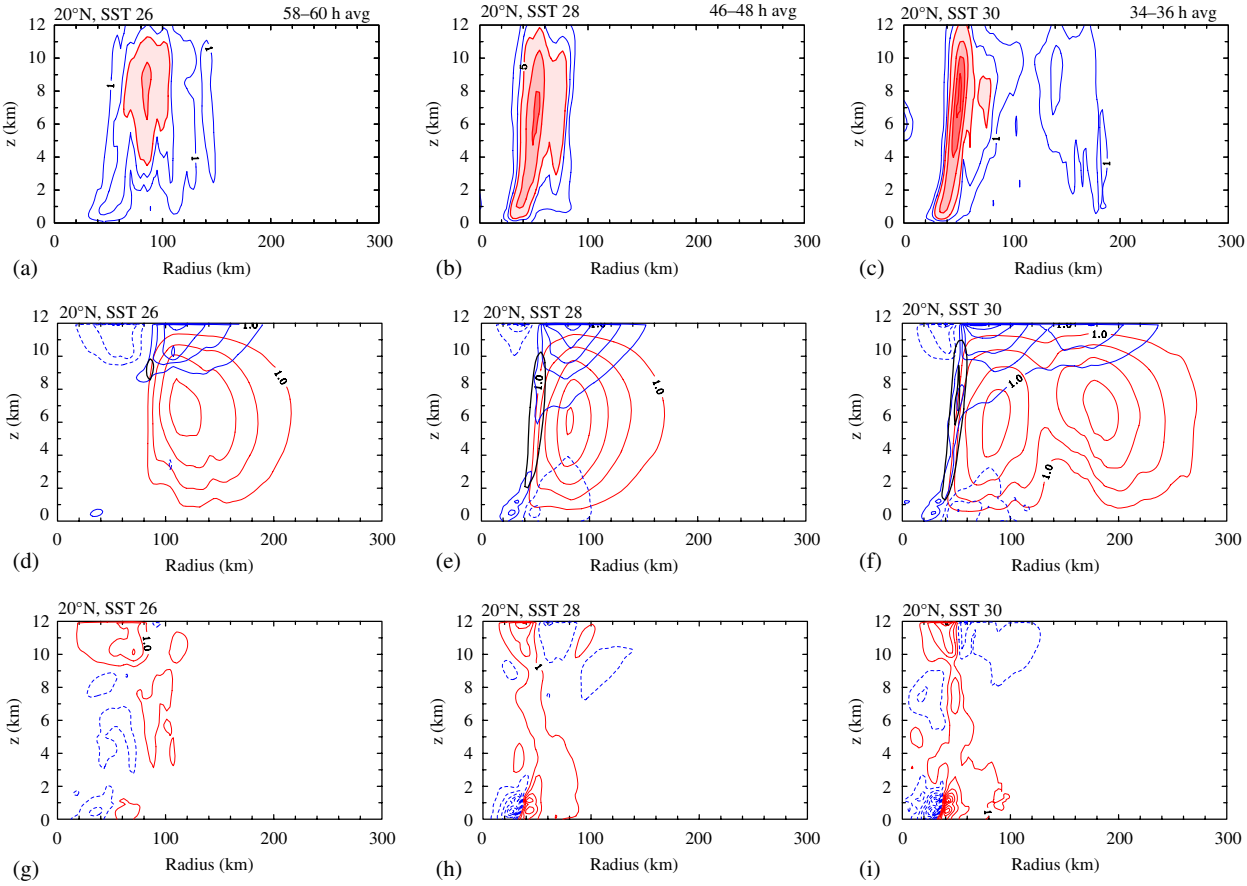

Figure 6. Radius–height plots of the time-averaged diabatic heating rate, based on azimuthally averaged fields from the CM1 calculations at 20°N for SST values of (a) 26 °C, (b) 28 °C and (c) 30 °C. The contour interval for blue contours is 2 K h^{-1} starting with the contour 1 K h^{-1}. The contour interval for red contours is 5 K h^{-1}, values between 5 and 10 K h^{-1} are shaded light pink, values between 10 and 15 K h^{-1} are shaded light red and values greater than 15 K h^{-1} are shaded darker red. Panels (d), (e) and (f) show the corresponding streamfunction of the balanced secondary circulation obtained by solving the Sawyer–Eliassen equation with these heating rates as forcing terms (red contours, contour interval 1 × 10 ^{8} kg s^{-1}). These panels show also the contours of radial wind speed (contour interval 1 m s^{-1}, positive values are solid blue, negative values are dashed blue) and vertical velocity (black contours, contour interval 0.5 m s^{-1}). Panels (g), (h) and (i) show the corresponding tendencies of the balanced tangential wind (contour interval 2 m s^{-1} h^{-1}, positive values are solid red, negative values are dashed blue).

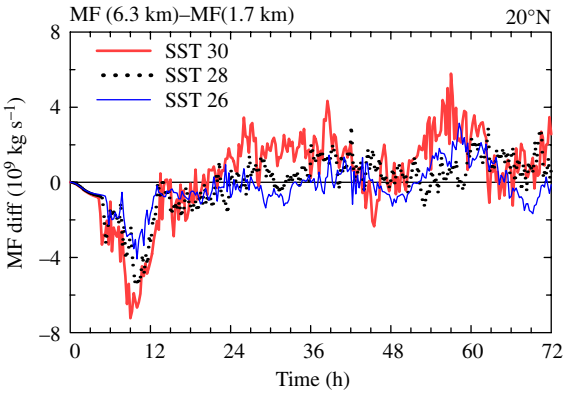

Figure 7. Time series of the difference between azimuthally averaged radially integrated mass flux in the middle troposphere at a height of 6.3 km and near the top of the boundary layer at 1.7 km in a series of CM1 calculations at the central latitude of 20°N for different SSTs (26 °C - thin solid blue curve, 28 °C - dotted black curve, 30 °C - thick solid red curve). These quantities are calculated by integrating the vertical mass flux, where it is positive, radially out to 300 km.

offered to explain the dependence of intensification rate on SST in section 4 are based on an axisymmetric perspective that would apply to the azimuthally averaged fields. More complete arguments would need to account also for eddy processes, as discussed in Persing *et al.* (2013) and Smith *et al.* (2015b).

6. Discussion

The foregoing study was motivated in part by a desire to help interpret observational data on tropical cyclone intensification rates. However, the focus is limited to one aspect of the problem, namely the effect of SST on intensification rate in comparison with the effects of latitude in the prototype problem for tropical cyclone intensification in a quiescent environment. Although the study uses a three-dimensional numerical model with an explicit representation of deep convection, only warm rain processes are considered. Ice microphysical processes are not taken into account and the effects of vertical wind shear, which are undeniably important in the real atmosphere, are not examined. We would not expect the interpretations of the quantitative differences in intensification rate for different SSTs to be modified appreciably if a parametrization scheme for ice microphysics were implemented, but one cannot be sure without performing the relevant calculations. Certainly, the neglect of vertical wind shear is a limitation in being able to provide a complete explanation of the observations and might be a factor in Hendricks *et al.*'s (2010) observational finding that '... the rate of intensification is not critically dependent on SST'. Because of the multiple factors that can affect the intensification rate of real storms, it is beyond the scope of the present work to try to reconcile the various observational studies.

7. Conclusions

We have examined the effects of changing the SST on the intensification rate of tropical cyclones at different latitudes. The study complements and extends the results of a recent study examining the latitudinal dependence only in the prototype problem for tropical cyclone intensification.

For a given SST, the results confirm the findings of Smith *et al.* (2015a) that intensification begins earlier and the intensification

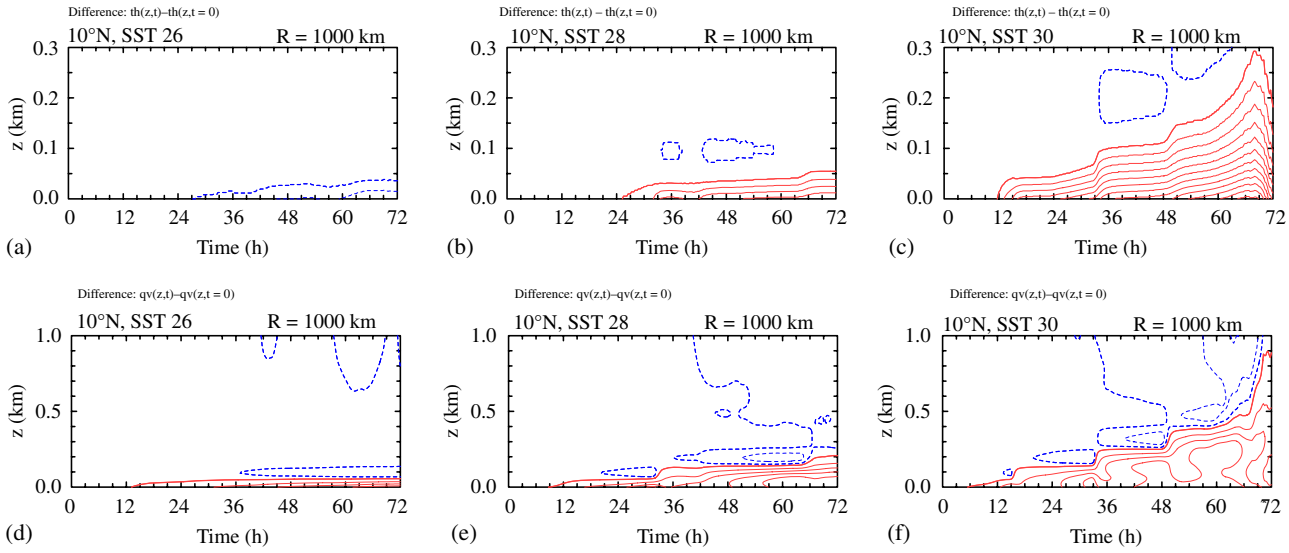

Figure 8. (a)–(c) Time–height diagrams of the difference between azimuthally averaged potential temperature at time t and that at the initial time ($t = 0$ h) in the lowest 0.3 km, at a radius of 1000 km from the geometrical domain centre. Solid red contours indicate positive values, dashed blue contours indicate negative values. The contour interval is 0.1 K. The solid red contour is 0.1 K, the dashed blue contour is −0.1 K. (d)–(f) Same diagrams, except for the water-vapour mixing ratio difference in the lowest 1.0 km. The first positive contour is 0.1 g kg^{-1} (solid red contour); the contour interval is 0.5 g kg^{-1} for positive values. The first negative contour is −0.1 g kg^{-1} (dashed blue contour); the contour interval is 0.2 g kg^{-1} for negative values. Shown are the results for the CM1 calculations at latitude 10°N. The interpolated data in the upper panels are based on information at four model levels and those in the lower panels are based on eight model levels.

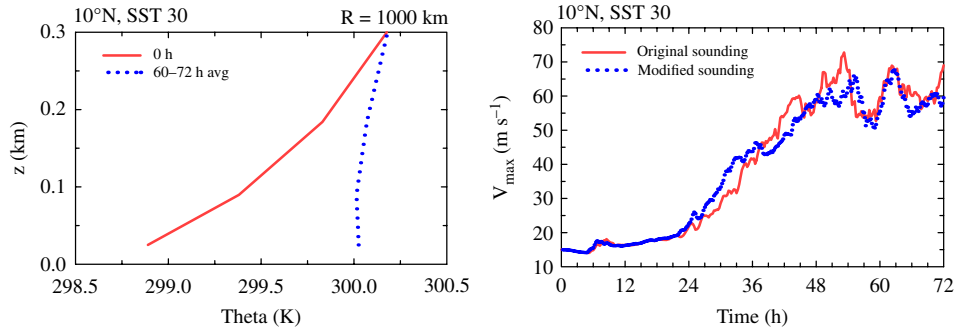

Figure 9. (a) Potential temperature profile in the lowest 0.3 km at a radius of 1000 km (azimuthally averaged) for the CM1 calculation at latitude 10°N and with an SST of 30 °C. The solid red curve shows the profile at the initial time, the dotted blue curve shows the profile averaged over the last 12 h of calculation (60–72 h avg). (b) Time series of maximum azimuthally averaged tangential wind speed for the two simulations at latitude 10°N and with an SST of 30 °C. The solid red curve shows the evolution of v_{max} in the 'original' (control) experiment. The dotted blue curve shows the evolution of v_{max} in the simulation where the 60–72 h averaged ambient profile at a radius of 1000 km from the control experiment was used as the initial environmental sounding.

rate increases as the latitude is decreased. However, they show important quantitative differences in the latitudinal dependence of intensification rate as the SST is changed. Specifically, the dependence on latitude is largest when the SST is marginal for tropical cyclone development (26 °C) and becomes less important as the SST is increased. For example, at 20°N or 30°N latitude, cyclone intensification is more strongly dependent on the SST than at 10°N.

Furthermore, we have shown that, at a fixed latitude, vortex intensification begins earlier and is more rapid as the SST is

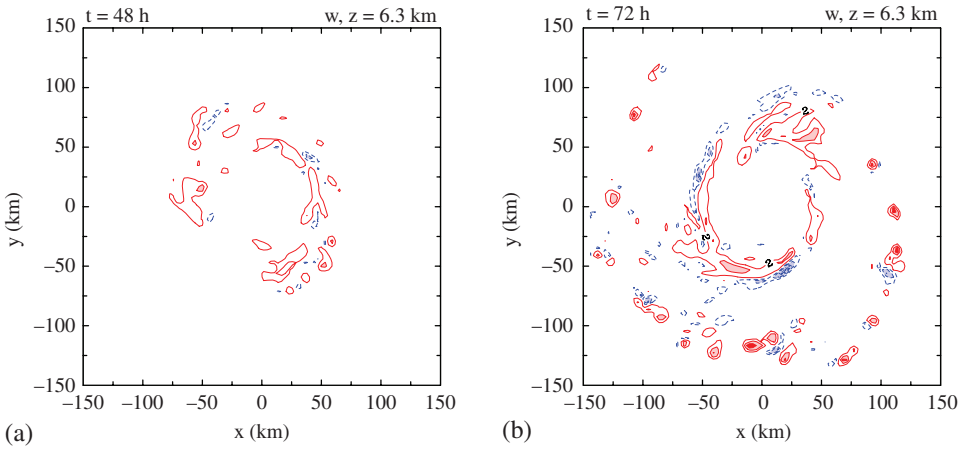

Figure 10. Horizontal cross-sections of vertical velocity at a height of 6.3 km in the CM1 calculation corresponding to latitude 20°N and an SST of 28 °C at (a) 48 h and (b) 72 h. Solid red contours indicate positive values. The interval for positive contours is 4 m s^{-1}, starting with the value of 2 m s^{-1}. Values between 6 and 10 m s^{-1} are shaded pink, values greater than 10 m s^{-1} are shaded red. Dashed blue contours indicate negative values. The interval for negative contours is 2 m s^{-1}, starting with −2 m s^{-1}. Values lower than −4 m s^{-1} are shaded light blue.

increased. An explanation for this behaviour is offered in terms of the classical axisymmetric paradigm for tropical cyclone spin-up. In brief, an increase in the SST is accompanied by a significant increase in the surface water vapour fluxes and corresponding increases in the low-level moisture and equivalent potential temperature. Where boundary-layer air is lofted into the vortex above, these increases lead to a larger radial gradient of diabatic heating in the low to middle troposphere and thereby to a stronger diabatically forced overturning circulation. The stronger inflow draws absolute angular momentum surfaces inwards at a higher rate, leading to faster spin-up.

The difference between the radially integrated vertical mass fluxes in the middle troposphere and at the top of the boundary layer can be used as another indicator of the strength of the inner-core deep convection. We showed that, at 20° latitude, this difference increases with increasing SST, an indication that, collectively, deep convection has a progressively greater ability to ventilate the air that is converging in the boundary layer as the SST is increased.

The foregoing explanations are based on an azimuthally averaged perspective, but the flow exhibits significant departures from axial symmetry, especially during the rapid intensification phase. The non-axisymmetric features, which are a prominent feature of real storms also, are discussed briefly, but remain a topic for future research.

Extension of the present study to examine the additional effects of vertical shear, mid-tropospheric dry air and ice microphysics would appear to be a fruitful avenue for future research.

Acknowledgements

The impetus for this study arose from discussions with John Kaplan during a visit by the second author to the Hurricane Research Division of NOAA in the autumn of 2014. We thank John Kaplan for his insightful comments on a pre-submission draft of the manuscript. NČ acknowledges support of a stipendium from Slovene Human Resources Development and Scholarship Fund. RKS and GK acknowledge financial support for this research from the German Research Council (Deutsche Forschungsgemeinschaft) under Grant number SM30/23-4 and the Office of Naval Research Global under Grant No. N62909-15-1-N021.

References

Bryan GH, Fritsch JM. 2002. A benchmark simulation for moist nonhydrostatic numerical models. *Mon. Weather Rev.* **130**: 2917–2928.

Bui HH, Smith RK, Montgomery MT, Peng J. 2009. Balanced and unbalanced aspects of tropical-cyclone intensification. *Q. J. R. Meteorol. Soc.* **135**: 1715–1731.

Dunion JP. 2011. Rewriting the climatology of the tropical North Atlantic and Carribean sea atmosphere. *J. Clim.* **24**: 893–908.

Emanuel KA. 1994. *Atmospheric Convection*. Oxford University Press: Oxford, UK.

Hendricks EA, Peng MS, Fu B, Li T. 2010. Quantifying environmental control on tropical cyclone intensity change. *Mon. Weather Rev.* **138**: 3243–3271.

Kaplan J, DeMaria M. 2003. Large-scale characteristics of rapidly intensifying tropical cyclones in the North Atlantic Basin. *Weather and Forecasting* **18**: 1093–1108.

Kaplan J, DeMaria M, Knaff JA. 2010. A revised tropical cyclone rapid intensification index for the Atlantic and Eastern North Pacific Basins. *Weather and Forecasting* **25**: 220–241.

Montgomery MT, Smith RK. 2014. Paradigms for tropical cyclone intensification. *Aust. Meteotrol. Ocean Soc. J. (Bruce Morton Memorial Volume)* **64**: 37–66.

Montgomery MT, Persing J, Smith RK. 2015. Putting to rest WISHE-ful misconceptions. *J. Adv. Model. Earth Syst.* **7**: 92–109, doi: 10.1002/2014MS000362.

Nguyen SV, Smith RK, Montgomery MT 2008. Tropical-cyclone intensification and predictability in three dimensions. *Q. J. R. Meteorol. Soc.* **134**: 563–582.

Ooyama KV. 1969. Numerical simulation of the life cycle of tropical cyclones. *J. Atmos. Sci.* **26**: 3–40.

Persing J, Montgomery MT, McWilliams J, Smith RK. 2013. Asymmetric and axisymmetric dynamics of tropical cyclones. *Atmos. Chem. Phys.* **13**: 12 299–12 341.

Rotunno R, Emanuel KA. 1987. An air–sea interaction theory for tropical cyclones. Part II evolutionary study using a nonhydrostatic axisymmetric numerical model. *J. Atmos. Sci.* **44**: 542–561.

Shapiro LJ, Willoughby H. 1982. The response of balanced hurricanes to local sources of heat and momentum. *J. Atmos. Sci.* **39**: 378–394.

Shin S, Smith RK. 2008. Tropical-cyclone intensification and predictability in a minimal three-dimensional model. *Q. J. R. Meteorol. Soc.* **134**: 1661–1671.

Smith RK. 2006. Accurate determination of a balanced axisymmetric vortex. *Tellus* **58A**: 98–103.

Smith RK, Montgomery MT. 2012. Observations of the convective environment in developing and non-developing tropical disturbances. *Q. J. R. Meteorol. Soc.* **138**: 1721–1739.

Smith RK, Montgomery MT. 2015. Towards clarity on tropical cyclone intensification. *J. Atmos. Sci.* **72**: 3020–3031.

Smith RK, Kilroy G. Montgomery MT. 2015a. Why do model tropical cyclones intensify more rapidly at low latitudes? *J. Atmos. Sci.* **72**: 1783–1804.

Smith RK, Zhang J, Montgomery MT. 2015b. The dynamics of intensification in an HWRF simulation of Hurricane Earl (2010) *Q. J. R. Meteorol. Soc.* Submitted.

